PERGAMON

International Journal of Heat and Mass Transfer 43 (2000) 399–415

International Journal of HEAT and MASS TRANSFER

www.elsevier.com/locate/ijhmt

Three-dimensional conjugate heat transfer in the microchannel heat sink for electronic packaging

Andrei G. Fedorov, Raymond Viskanta*

Heat Transfer Laboratory, School of Mechanical Engineering, Purdue University, West Lafayette, IN 47907, USA

Received 15 January 1999; received in revised form 12 April 1999

Abstract

A three-dimensional model is developed to investigate flow and conjugate heat transfer in the microchannel-based heat sink for electronic packaging applications. The incompressible laminar Navier–Stokes equations of motion are employed as the governing conservation equations which are numerically solved using the generalized single-equation framework for solving conjugate problems. The theoretical model developed is validated by comparing the predictions of the thermal resistance and the friction coefficient with available experimental data for a wide range of Reynolds numbers. The detailed temperature and heat flux distributions as well as the average heat transfer characteristics are reported and discussed. The analysis provides a unique fundamental insight into the complex heat flow pattern established in the channel due to combined convection–conduction effects in the three-dimensional setting. Important practical recommendations are also provided regarding the cooling efficiency of the microchannel heat sinks as well as a possible failure due to the thermal stresses induced by the extremely large temperature gradient at the entrance of the channels.

1. Introduction

Design of the efficient and compact heat dissipation devices is paramount to sustaining a continuous growth at almost a geometric progression rate in performance of the leading-edge microelectronic products [1]. Reference is made to this recent account for a more comprehensive citation of relevant literature. The electronic packages typically operate at very high average heat fluxes (10 and 25 W/cm^2 for plastic DIP and ceramic PGA, respectively) [1,2] and, for stable and reliable operation, must be maintained at the temperature below 130°C. Chu and Chrysler [1] provide an overview of the state-of-the-art cooling techniques that are currently employed by the semiconductor industry for heat dissipation in everything from the mainframe to portable computers. These include the extended surfaces (fins) with turbulators, the highly parallel air and liquid impingement systems, modular internal conduction enhancement, indirect and direct liquid cooling with water and dielectric coolants, respectively, and, finally, the special cooling systems such as the heat pipes and liquid metal heat sinks.

During the last decade, several novel cooling schemes have been proposed and extensively studied both experimentally and theoretically. In particular, Bowers and Mudawar [3] showed that the cooling scheme employing two-phase flow in mini-channels is capable of removing the record high heat fluxes generated by the electronic packages. However, the possible instability of the system when operating close to the CHF point is reducing considerably the advantages of two-phase cooling schemes for practical applications.

* Corresponding author. Tel.: +765-494-5632; fax: +765-494-0539.

E-mail address: viskanta@ecn.purdue.edu (R. Viskanta)

0017-9310/00/$ - see front matter
PII: S0017-9310(99)00151-9

Nomenclature

C	friction coefficient constant
c_p	specific heat at constant pressure
D_h	hydraulic diameter
f	friction coefficient
H_y, H_z	width of the channel in y- and z-directions, respectively (see Fig. 1)
Kn	Knudsen number, λ/D_h
k	thermal conductivity
L	length of the channel (see Fig. 1)
p	pressure
q	heat flux
q^*	modified logarithmic heat flux, $\text{sign}(q)\ln\lvert q\rvert$
R_t	thermal resistance
Re	Reynolds number, $\rho u_0 D_h/\mu$
T	temperature
u, v, w	velocity components in x-, y-, and z-directions, respectively
W_y^l, W_y^r	thickness of the channel walls in y-direction (see Fig. 1)
W_z^l, W_z^r	thickness of the channel walls in z-direction (see Fig. 1)
x, y, z	Cartesian coordinates (see Fig. 1)

Greek symbols

Γ	generalized diffusion coefficient in Eq. (5)
μ	dynamic viscosity
ρ	density

Subscripts

b	refers to bulk
g	refers to gas/fluid
i	refers to input
w	refers to wall/solid
0	refers to inlet

Superscripts

l	refers to left (negative coordinate direction in Fig. 1)
r	refers to right (positive coordinate direction in Fig. 1)

Another valuable alternative comes from the use of a porous media as the heat sink, due to a drastic increase in the specific surface area available for heat removal [4–8]. The major drawbacks associated with the use of the porous media for enhancing heat transfer are: a substantial increase in the pressure drop; very strict requirements for the coolant purity to avoid pore clogging; and eventual appearance of the hot spots in the package.

Recent advances in microfabrication techniques have led to revival of the concept of the ultra-compact microchannel heat exchangers for electronic cooling which was originally introduced by Tuckerman and Pease [9,10]. In principle, such microchannels can be machined at the back of a substrate of electronic chips and, therefore, can reduce the internal (contact) thermal resistance of the heat sink practically to zero. The cooling rates in such microchannel heat exchangers should increase significantly due to a decrease in the convective resistance to heat transport caused by a drastic reduction in the thickness of thermal boundary layers. The overall excellent potential capacity of such a heat sink for heat dissipation is based on the large heat transfer surface-to-volume ratio of the microchannel heat exchangers.

The flow and heat transfer in microchannels have become a subject of growing research attention since the early 1990s. Several pioneering experimental studies [11–13] found significant deviation of the flow parameters in the microchannels compared to those in the conventional 'large' channels. In particular, the authors reported a decrease in the friction factor for the gas flow in the microchannels relative to its value predicted using standard correlations for laminar flow. The review of these works has been recently presented by Peng and Wang [14]. In contrast, Webb and Zhang [15] claim that the accepted single-phase flow correlations adequately predict their experimental data for round and rectangular tubes with hydraulic diameter of the order of 1 mm. Furthermore, as Nakayama et al. [16] have pointed out, the geometric precision and tolerance control in the experimental assembly is often beyond the manual skills of the experimenter, and this leads to the considerable experimental uncertainty and inconsistencies in the reported measurements. Unfortunately, we were able to identify only few papers [17–19] that provide the experimental data for friction and heat transfer in the microchannels under conditions which are directly relevant to those found in the integrated circuits of modern electronic devices, i.e., when the substrate (heat spreader) is highly conducting and massive in comparison to channel dimensions and, therefore, the conjugate conduction–convection effects are important.

Few attempts have been made to analyze the microchannel flows and heat transfer, theoretically. In particular, Weisberg et al. [20] numerically analyzed a conjugate heat transfer problem in the microchannel

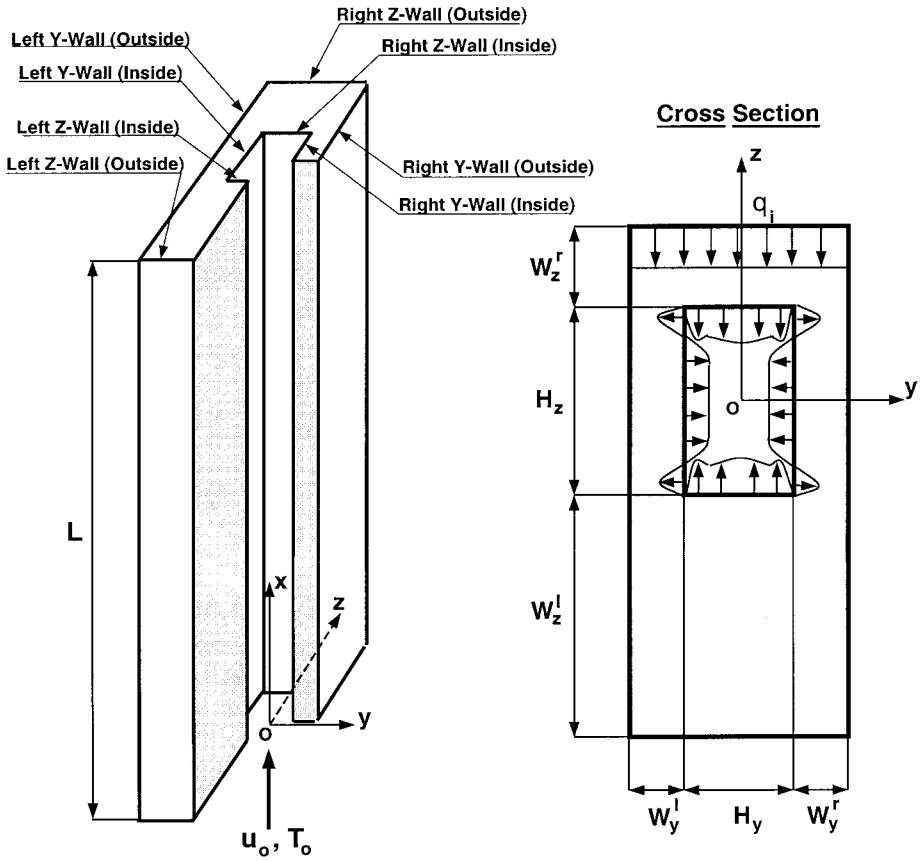

Fig. 1. Schematic of the physical arrangement and the coordinate system.

heat exchanger. Yu et al. [21] performed a scale analysis of the flow and heat transfer characteristics in microtubes. Several new theoretical models were also proposed recently in order to describe the peculiar features of the microscale flow and heat transfer. Li et al. [22,23] utilized the kinetic theory of gases to derive the effective fluid transport properties close to the wall surface and, then, to obtain analytical expressions for the friction factor and the Nusselt number. Mala et al. [24] and Yang et al. [25] included the surface electrokinetic effects in the analysis of the flow and heat transfer in microchannels. However, due to the lack of a clear fundamental understanding of the transport mechanisms on microscale, most of these theories appear to be rather speculative and, therefore, have not gained a wide acceptance [14]. Chen et al. [26] studied the possibility of using the Navier–Stokes equations for compressible gas in continuum flow formulation together with the slip and non-slip boundary conditions in order to describe gas flow in microchannels. Recently, Fedorov and Viskanta [27] extended the efforts to analyze the transient dynamics of conjugate heat and mass transfer in microchannels in the presence of the surface chemical interactions.

It is clear that successful design of the microchannel-based heat sinks requires fundamental understanding of the transport processes occurring on the microscale. Detailed measurements and predictions of the local temperature and heat fluxes are critically important for development of the compact, efficient, and reliable systems for thermal management. In this paper, we employ the numerical simulations to gain insight into combined convection–conduction heat transfer in the rectangular silicon microchannel, which is a unit cell of the experimental electronic heat sink. To this end, the system of three-dimensional Navier–Stokes equations for conservation of mass, momentum, and energy based on the continuum flow assumption is used as a mathematical model of the process. First, the validity of the developed mathematical model is critically assessed by comparing the theoretical predictions with available measurements of the friction factor coefficient and thermal resistance in the microchannel heat sink [19]. Then, the local temperatures and heat fluxes are

analyzed with the aim to identify the heat flow pattern established in the microchannel under the strong influence of three-dimensional conjugate effects. Finally, the average heat transfer characteristics are also obtained, and important practical recommendations are provided regarding the overall heat sink performance and possible locations of the structural failure due to excessive thermal gradients.

2. Analysis

2.1. Physical model, model equations, and boundary conditions

Consider a three-dimensional asymmetric rectangular channel shown schematically in Fig. 1. The channel geometry is the same as the one which was employed in the experimental work by Kawano et al. [19]. A theoretical model for flow and conjugate heat transfer in the microchannel is developed under the following assumptions:

1. the hydraulic diameter of microchannels under development is about 100 μm and is expected to decrease to 10 μm. This yields a typical Knudsen number[1] for water as a coolant to be between 3.5×10^{-5} and 3.5×10^{-4} which lies in the continuous flow regime ($Kn < 10^{-3}$) [28]. Hence, the conservation equations based on the continuum model (Navier–Stokes equations of motion) can still be used to describe the transport processes
2. the transport processes are considered to be steady-state and three-dimensional
3. the flow is incompressible and laminar
4. thermal radiation is neglected in comparison to advection (the typical operation temperature is below 100°C)
5. the development of the flow and temperature fields at the inlet of the channel is carefully resolved since it is the region where the largest temperature gradients and, therefore, thermal stresses are expected to occur
6. the thermophysical properties are temperature dependent.

Under the stated assumptions, the conservation equations of mass, momentum, and energy for the fluid and the solid channel walls can be written as follows [28] (see Fig. 1 for coordinate system):

Conservation of mass (continuity)

$$\nabla\left(\rho\vec{V}\right) = 0 \tag{1}$$

Conservation of momentum

$$\vec{V}\cdot\nabla\left(\rho\vec{V}\right) = -\nabla p + \nabla\cdot\left(\mu\nabla\vec{V}\right) \tag{2}$$

Conservation of energy for fluid

$$\vec{V}\cdot\nabla\left(\rho c_p T_{\mathrm{g}}\right) = \nabla\cdot\left(k_{\mathrm{g}}\nabla T_{\mathrm{g}}\right) \tag{3}$$

Conservation of energy for solid

$$\nabla(k_{\mathrm{w}}\nabla T_{\mathrm{w}}) = 0 \tag{4}$$

In the absence of a unique and well-established methodology for scaling of combined convection–conduction heat transfer in the three-dimensional conjugate problems, no attempt is made to non-dimensionalize the governing conservation equations.

A uniform heat flux (q_{i}) is imposed as a boundary condition at the heated right Z-wall ($z = H_z/2 + W_z^r$) while all other outside walls of the channel (in x-, y-, and z-directions) are taken to be perfectly insulated (see Fig. 1). The velocity (u_0) and temperature (T_0) of the fluid entering the channel are specified, while the gradients of the temperature and velocity components are set to vanish at the exit of the channel. A no-slip boundary condition is imposed on the velocity components at the walls inside the channel. Finally, the continuity of the temperature and heat flux are used as the conjugate boundary conditions to couple the energy equations for the fluid and solid phases.

2.2. Method of solution

The model conservation equations (all, but continuity) are initially expressed in the general form with a transient term included as the iteration parameter,

$$\frac{\partial}{\partial t}(\rho\phi) + \frac{\partial}{\partial x_i}(\rho u_i\phi) = \frac{\partial}{\partial x_i}\left(\Gamma\frac{\partial\phi}{\partial x_i}\right) + S \tag{5}$$

where ϕ represents any dependent variable, i.e., velocity components and temperature, and Γ is the general diffusion coefficient. A fully implicit, absolutely stable Euler method with very large time steps is employed to integrate Eq. (5) in time, until the steady-state solution is achieved. The governing partial differential equations along with the boundary conditions are discretized over the spatial coordinates by means of the control volume integration technique [29]. The resulting finite-difference approximation of derivatives

[1] The Knudsen number, $Kn = \lambda/D_{\mathrm{h}}$, defines the relative magnitude of the mean free path of the fluid molecules λ in respect to the characteristic dimension (hydraulic diameter D_{h}) of the channel. The mean free path λ depends on the density, temperature, and viscosity of the fluid and is equal to $\mu\sqrt{\pi}/\sqrt{2\rho^2 RT}$.

Table 1
Geometrical dimensions of the unit cell

H_z (μm)	H_y (μm)	W_z^l (μm)	W_z^r (μm)	W_y^l (μm)	W_y^r (μm)
180	57	450	270	21.5	21.5

produces a system of linear algebraic equations which are then solved by using a line-by-line iterative method. The method solves a line of nodes by applying the three-diagonal matrix inversion algorithm and sweeps the domain of the integration in different directions along the coordinate axes. The SIMPLER algor-

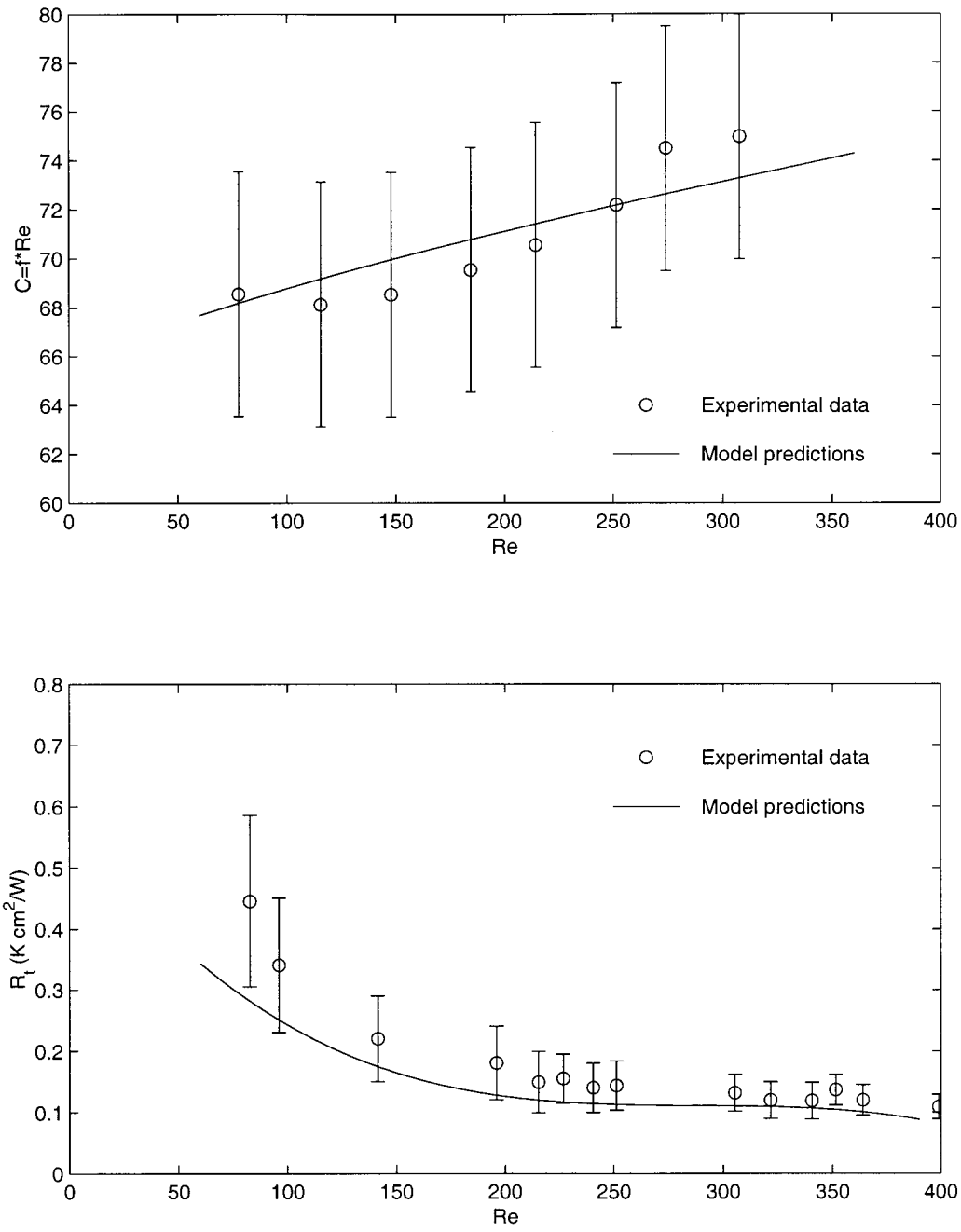

Fig. 2. Comparison of the theoretical predictions and experimental data [19] of the friction coefficient Poiseuille constant and the convective thermal resistance at the exit for the water flow in the silicon microchannel.

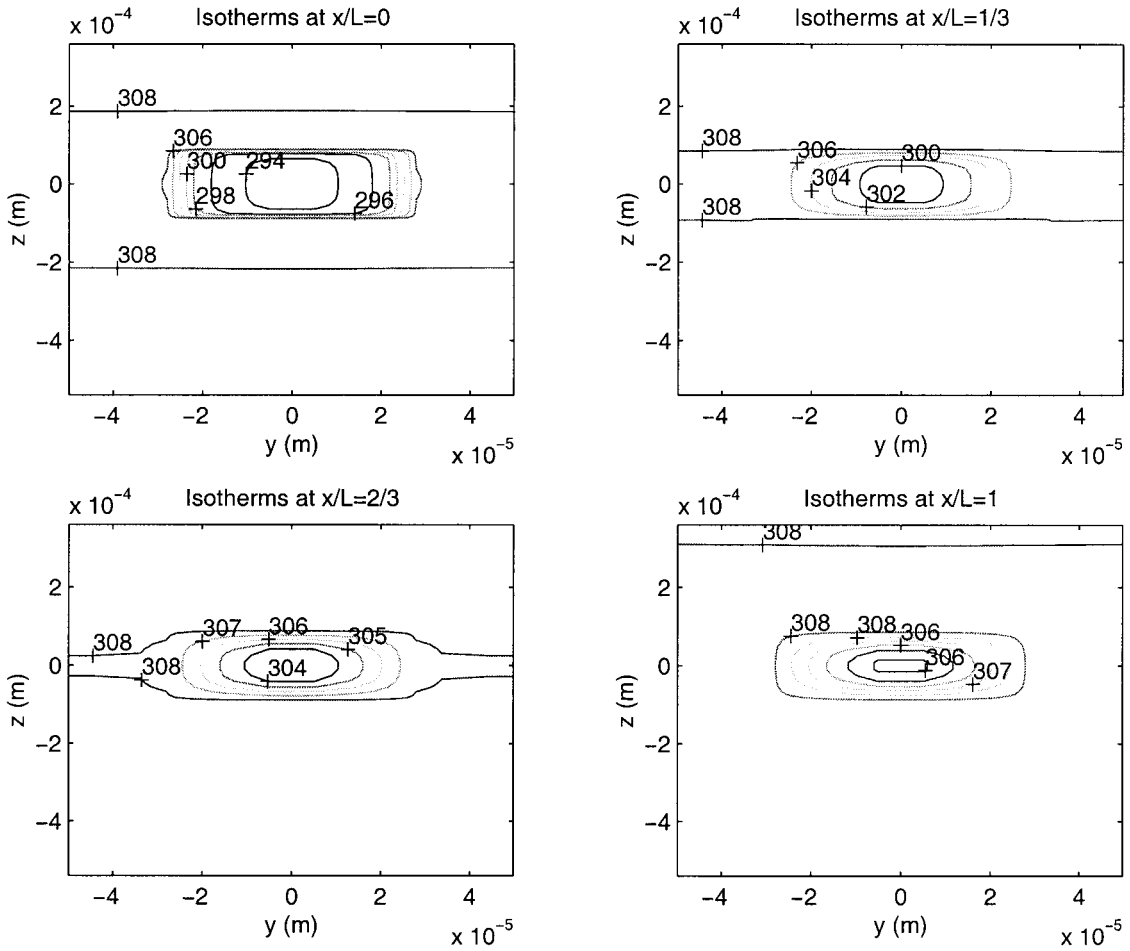

Fig. 3. Temperature distributions (in Kelvins) at four different cross-sections along the channel.

ithm is employed to solve the coupled system of conservation equations in primitive or dimensional variables, and this is discussed in detail by Patankar [29]. Suffice it to mention that the fluid and solid energy equations, (3) and (4), are combined into a single equation by using the appropriate values for the velocity components ($u = v = w = 0$ within the wall) and thermophysical properties in the corresponding regions of the channel. The solution of the model equations is then achieved by inter-system iterations between the momentum and global energy conservation equations at each time step. The iterations are terminated when the steady state is reached and the global energy and mass balances are satisfied within $1.0 \times 10^{-3}\%$.

A highly compressed nonuniform grid near the channel walls was adopted in order to properly resolve viscous shear layers. Sine-in-power distribution was shown to be very reliable even for the turbulent shear flows at relatively high Reynolds numbers [30] and, therefore, is used in this study. The grid nodes were also concentrated along the axial direction in the entrance of the channel for the proper resolution of the flow and thermal development regions. Additional details regarding the mesh size and the node distribution are given in the following section.

3. Results and discussion

3.1. Model validation

The numerical algorithm and computer program were carefully evaluated by comparing model predictions with available experimental data for friction and conjugate heat transfer in the microchannels [19]. The test section of the experimental heat exchanger had 110 identical silicon microchannels, so that the unit cell of the heat exchanger can be represented by the asymmetric rectangular channel as shown in Fig. 1. The channel length was 10 mm and the geometrical

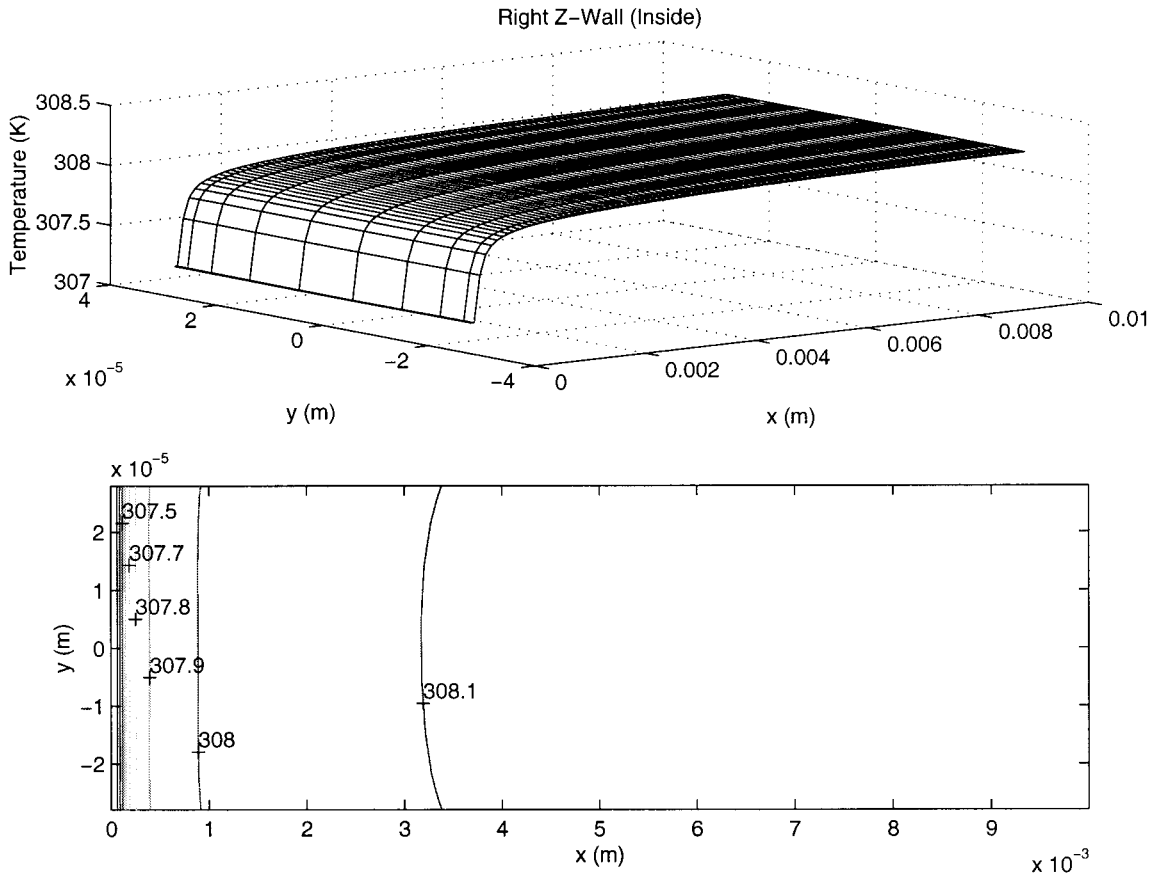

Fig. 4. Temperature distribution (in Kelvins) at right Z-wall inside the channel.

dimensions of the unit cell cross-section are summarized in Table 1 (see Fig. 1 for notation). In the experiments, water was used as a working fluid with the inlet temperature (T_0) = 20°C. An approximately uniform heat flux (q_i) of 90 W/cm^2 was imposed at the right outer Z-wall of the rectangular channel (see Fig. 1), while all other external surfaces were insulated. Further experimental details can be found in the original paper by Kawano et al. [19].

Fig. 2 compares the theoretically predicted and measured friction coefficient Poiseuille constant [$C = f \times Re$] and convective thermal resistance based on the outer right Z-wall temperature at the channel exit $\{R_t = [T_w(x = L, y = 0, z = H_z/2 + W_z^r) - T_0]/q_i\}$ for a wide range of the flow Reynolds numbers. It should be noted that the measurements and predictions of the Poiseuille constant C are reported for the case when the microchannel heat exchanger is not heated ($q_i = 0$).

Clearly, a good agreement between the model predictions and experimental data has been obtained. This is especially true in calculation of the friction coefficient Poiseuille constant where the theoretical results and the measurements are very close. The thermal resistance R_t appears to be slightly underpredicted, particularly at the smaller Reynolds numbers; however, it still lies within the range of the experimental uncertainties outlined by the error bars. The behavior of the Poiseuille constant C versus the Reynolds number deserves some additional remarks. The point is that the assumption of the fully developed Poiseuille flow, which is used in most studies of the microscale flow and heat transfer [14], appears to be rather questionable. Indeed, the Poiseuille theory predicts the constant value of the friction factor constant C regardless of the value of the Reynolds number [31], while the experimental data and our theoretical predictions show an approximately linear increase in C with an increase in Re. This is because, the length of the flow development region and, in turn, the value of the constant C in the Poiseuille friction law are linearly proportional to the Reynolds number [31]. For larger Reynolds numbers,

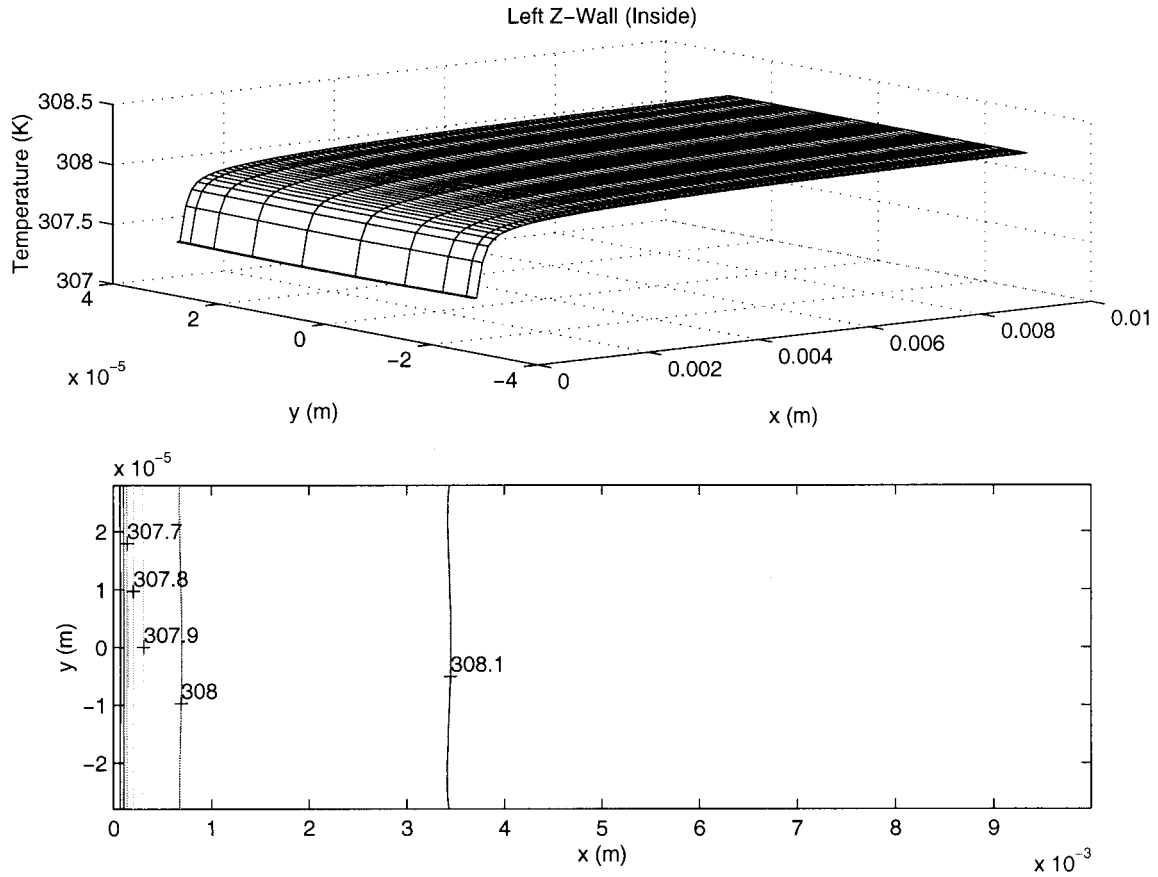

Fig. 5. Temperature distribution (in Kelvins) at left Z-wall inside the channel.

the development length can be significant relative to the channel length and, therefore, the Poiseuille flow assumption may lead to considerable error in the analysis.

Finally, the comparison of theoretical predictions with the experimental data was also used to assess the grid independence of the results. The CPU time as well as memory storage required for performing three-dimensional conjugate calculations increase dramatically as the number of grid nodes increases even slightly. This necessitated a search for the numerical grid with the smallest possible number of nodes but still satisfying the acceptable accuracy requirements. Different size meshes, ranging in total size from $60 \times 10 \times 20$ to $120 \times 20 \times 40$ in x-, y-, and z-directions, respectively, were employed in testing the numerical model. The results of the grid sensitivity study showed that the simulations based on the grid with 100 nodes in the x-direction, 16 nodes in the y-direction, and 32 nodes in the z-direction provide satisfactory numerical accuracy and are essentially grid independent. A further grid refinement produced a maximum incremental improvement of less than 0.1% in both local and average flow and heat transfer characteristics. It should also be mentioned that at least 3 nodes were placed in the thinnest Y-walls, and the maximum 6 nodes were placed in the thickest Z-walls (see Fig. 1).

The following three subsections are devoted to the detailed local and average results for the case of $Re = 140$, in order to foster a fundamental understanding of the microchannel flow and conjugate heat transfer in a truly three-dimensional geometry.

3.2. Local temperature distributions

Fig. 3 shows the contour plots of the isotherms at four different y–z cross-sections along the channel. The close analysis of the thermal field evolution indicates that the solid walls are essentially isothermal everywhere, while the isotherms within the fluid zone are initially very closely packed (see $x/L = 0$) and, then, gradually spread out with a simultaneous increase in the fluid core temperature (see $x/L = 1/3$, $2/3$, and 1). Three very important observations can be deduced

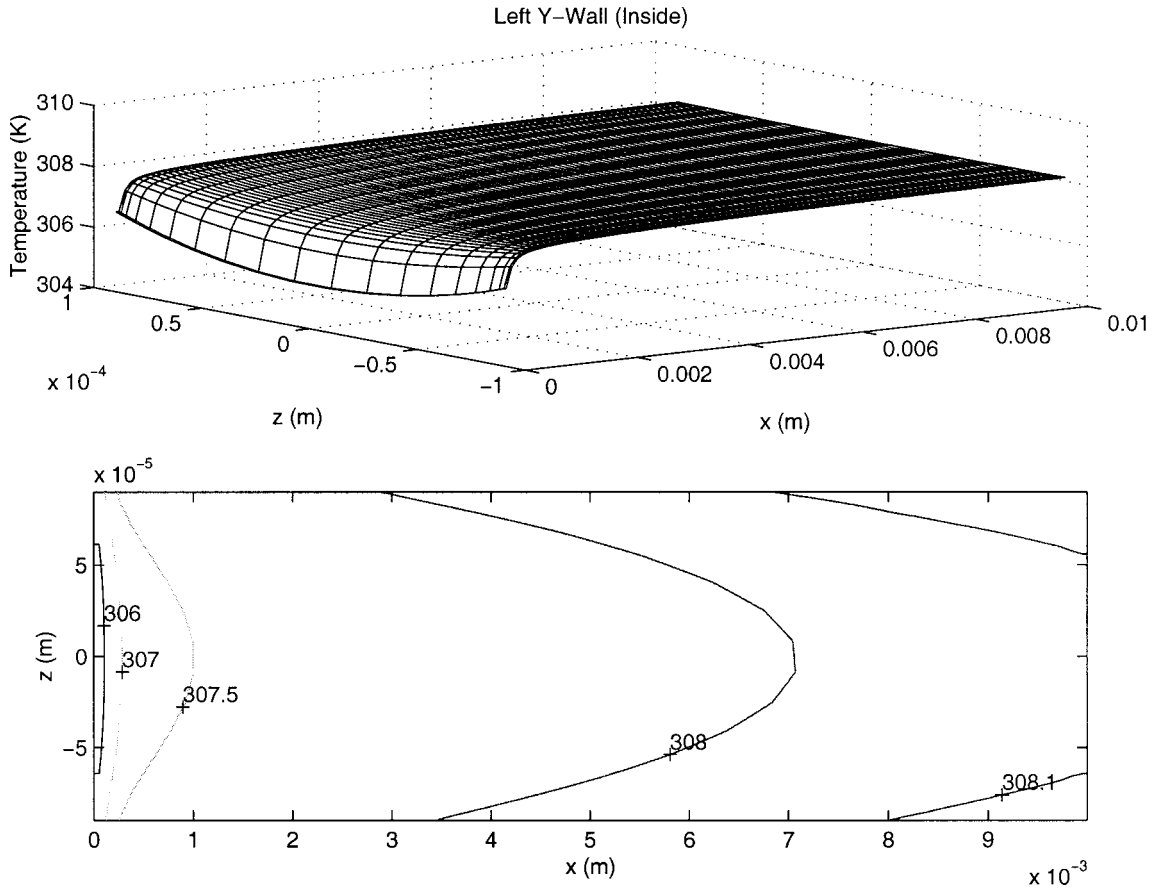

Fig. 6. Temperature distribution (in Kelvins) at left and right Y-walls inside the channel.

from the given temperature isopleths: (1) the intensity of heat transfer (heat fluxes) between solid and fluid is in its peak in the inlet portion of the channel; (2) the heat flux, imposed at the right Z-wall only, is immediately spread out by conduction within the silicon substrate and eventually is transferred to the fluid almost uniformly through all four inner walls of the channel; and (3) the thermal development region occupies essentially the entire length of the channel owing to the conjugate convection–conduction interactions.

Figs. 4–6 depict the spatial temperature distributions at the right Z-wall, at the left Z-wall, and at the left and right Y-walls inside the channel, respectively. As expected, the temperature of both the Z- and Y-walls increases sharply in the longitudinal x-direction very close to the channel inlet ($x/L < 0.1$) owing to a rapid decrease in the local convective heat transfer coefficient as the boundary layer thickness increases with development of the coolant flow. At the same time, the temperature of the Z-walls (Figs. 4 and 5) is essentially uniform in the transverse y-direction, whereas the temperatures of the left and the right Y-walls both inside (Fig. 6) and outside (Fig. 7) the channel vary noticeably in the transverse z-direction, at least for $x/L < 0.5$. The temperature of the left and right Z-walls outside the channel is virtually constant and, therefore, is not presented. Such temperature distributions at the inner and outer channel walls serve as an evidence of the very complex heat flow pattern established in the channel due to combined convective heat removal and three-dimensional conduction heat spreading in the microchannel heat sink. That is, the heat is introduced at the right Z-wall of the channel (see Fig. 1 for wall IDs), then it is efficiently spread by conduction to all four channel walls while being recirculated in the upstream direction and transferred to the coolant mostly in the inlet portion of the channel. This is where the convective resistance is the smallest. By this process, the longitudinal, upstream directed heat recirculation zones are created within the highly conducting walls of the channel which, in turn, lead to

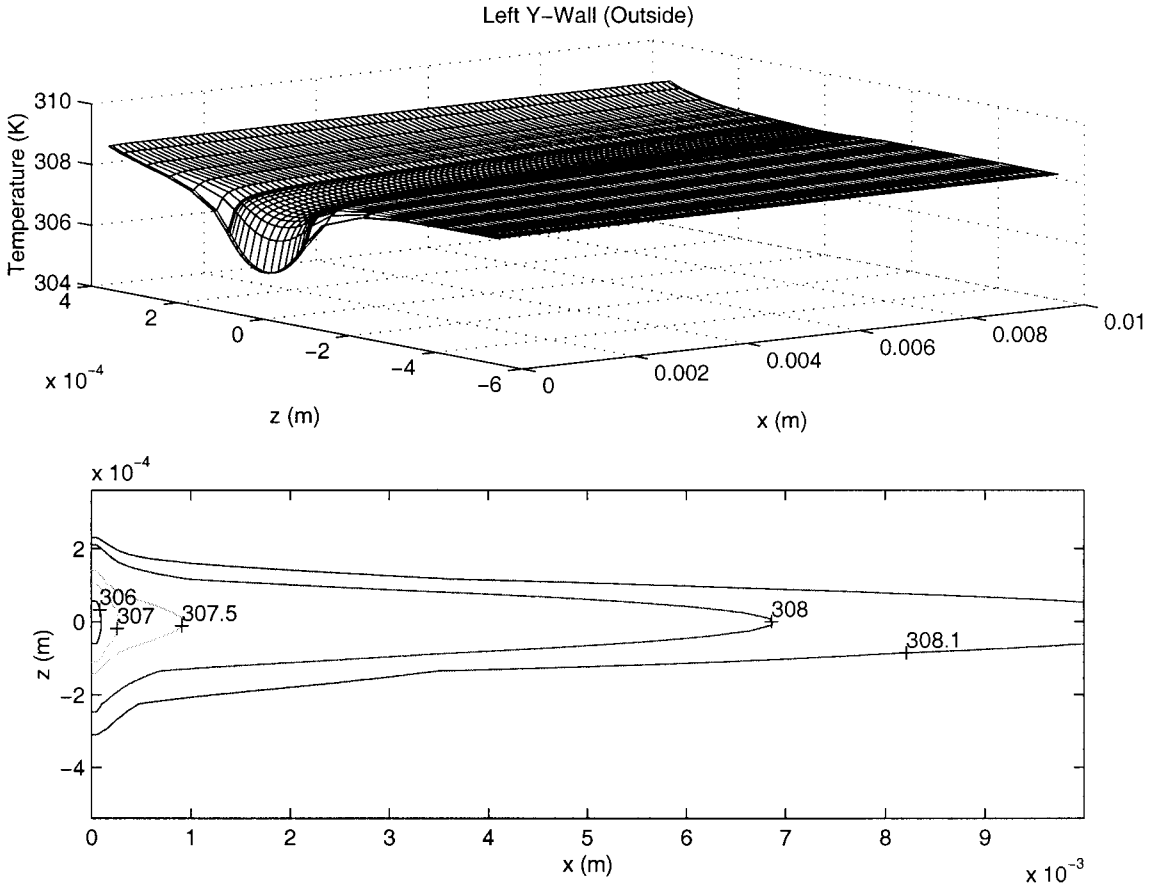

Fig. 7. Temperature distribution (in Kelvins) at left and right Y-wall outside the channel.

very large temperature gradients at the entrance of the heat sink.

3.3. Local heat flux distributions

In this subsection, the distributions of the local heat fluxes are presented at the inner walls of the channel where the solid and the fluid are in direct contact. The heat fluxes are taken to be positive if they are directed from the solid to the fluid, and negative, otherwise. Furthermore, the modified (logarithmic) wall heat flux $[q_w^* = \mathrm{sign}(q_w) \times \ln|q_w|]$ is used for the graphical presentation of results in order to accommodate several orders of magnitude variation in the local heat fluxes. To provide a baseline for analysis, the input heat flux ($q_i = 90$ W/cm^2 $= 90 \times 10^4$ W/m^2) corresponds to 13.7 in terms of the modified heat flux q_i^*.

The local heat fluxes at the channel walls, as shown in Figs. 8–10, confirm the overall physical picture of the heat transfer process implied by the analysis of local temperature fields in Section 2. Indeed, the local heat fluxes are the greatest in the inlet portion of the channel, and they decrease rapidly in the longitudinal x-direction. In contrast to the temperature distributions (see Section 2), the local heat fluxes at both the right and left Z-walls (Figs. 8 and 9, respectively) show significant variation in the transverse y-direction, unlike the fluxes at the right and left Y-walls (Fig. 10), which are nearly uniform everywhere but in the inlet and corner regions. Furthermore, the heat fluxes at the Y-walls are almost two orders of magnitude larger than those at the Z-walls. This is because the spacing between Y-walls (= 57 μm) is about three times smaller than that between Z-walls (= 180 μm). The small wall spacing means a thinner boundary layer and, in turn, much larger local convective heat transfer at Y-walls as compared to the Z-walls.

The same reasonings are valid everywhere but in the channel corners, where the convective heat transfer is a product of interactions between the boundary layers developed along both Y- and Z-walls. The direction and the magnitude of the heat flux in the corners are driven by competition between the two local thermal resistances: (i) the first defines the heat transport from

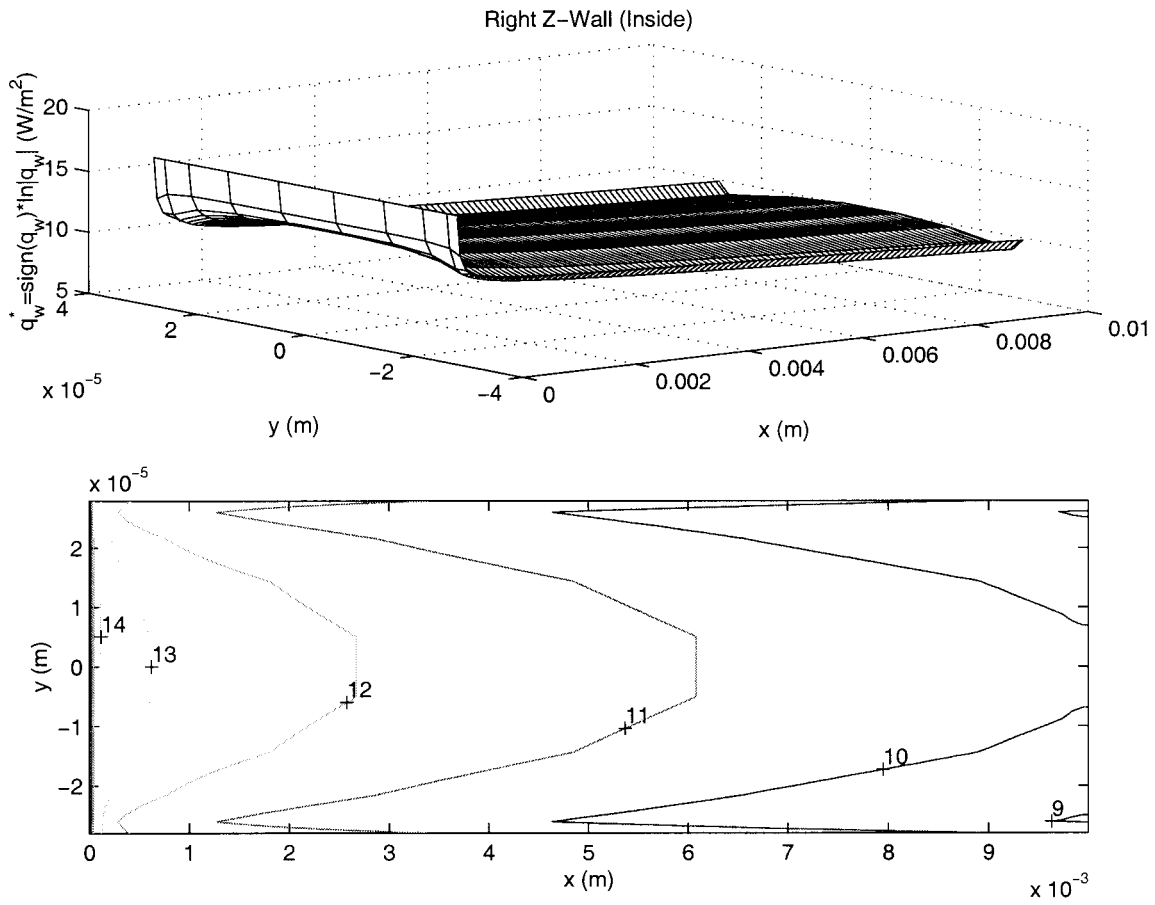

Fig. 8. Heat flux isopleths at right Z-wall inside the channel.

the wall through the boundary layer to the fluid core; and (ii) the second one quantifies the possibility of heat transport from one wall through the corner boundary layer to an adjacent wall. The importance of the second alternative pathway for the heat flow in the corners of the channel can be truly appreciated only in three-dimensional conjugate heat transfer problems.

In the present case, for example, the thermal resistance for heat conduction through the silicon is much smaller than the convective resistance for heat transfer through the fluid; therefore, the heat, transferred to the fluid in the corner area of the Z-walls, chooses the pathway with the least possible resistance (i.e., highly conducting solid walls) and bypasses through the fluid to enter the solid substrate in the corner area of the Y-walls instead of proceeding to the fluid core. The intricate heat flow structure with the heat 'vortices' in the corners, developed in the transverse y–z cross-sections of the channel, is sketched schematically in Fig. 1. Such a heat flow pattern produces the local negative (directed from the fluid to the solid) heat fluxes in the vicinity of corners of the Y-walls (see Fig. 10), even though the local Y-wall temperature is larger than the bulk fluid temperature. This means that the local heat transfer coefficient would also become negative if it were defined in terms of the conventional fluid bulk-to-wall temperature difference. Therefore, in general, the concept of the heat transfer coefficient cannot serve as a consistent framework for defining the local heat transfer rates in the conjugate problems.

3.4. Average and bulk characteristics

Fig. 11 depicts the fluid bulk temperature and the average temperatures of the Y- and Z-walls, as the functions of the longitudinal distance x, which are defined by

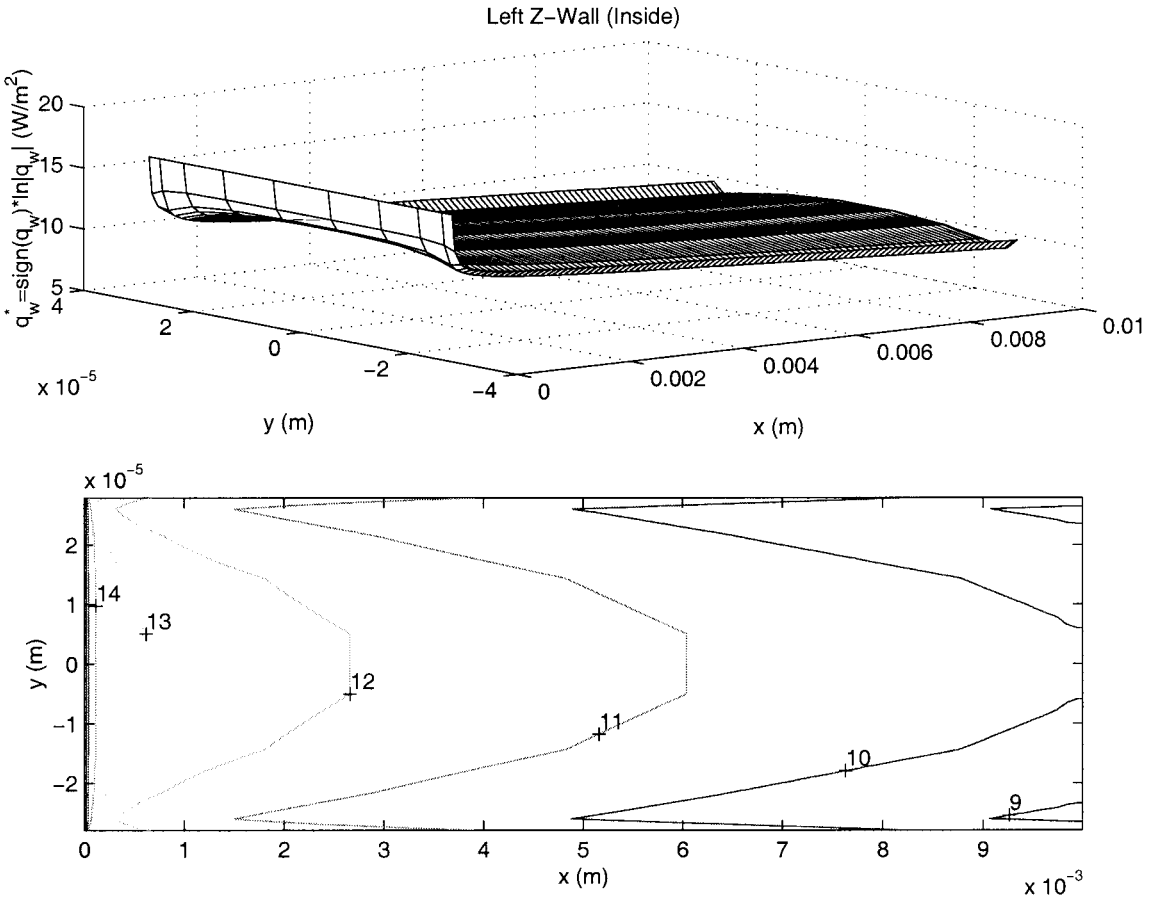

Fig. 9. Heat flux isopleths at left Z-wall inside the channel.

$$T_b(x) = \int_{-H_y/2}^{H_y/2} \int_{-H_z/2}^{H_z/2} \rho u c_p T(x, y, z)\, dz\, dy / \int_{-H_y/2}^{H_y/2} \int_{-H_z/2}^{H_z/2} \rho u c_p\, dz\, dy \quad (6)$$

$$\bar{T}_y(x) = \int_{-H_z/2}^{H_z/2} T\big(x, y = \pm H_y/2, z\big)\, dz / H_z \quad (7)$$

$$\bar{T}_z(x) = \int_{-H_y/2}^{H_y/2} T(x, y, z = \pm H_z/2)\, dy / H_y \quad (8)$$

Following the local temperatures, the average wall temperatures increase drastically within the small inlet portion of the channel ($x/L < 0.1$) due to an increase in the local convective thermal resistance. On the other hand, the fluid bulk temperature increases gradually along the x-direction, and it almost reaches the wall temperature at the exit of the microchannel. Overall, the average temperatures of both Z-walls are slightly larger than those of Y-walls owing to much smaller convective resistance for solid-to-fluid heat transfer for the closer spaced Y-walls. Furthermore, as expected, the average temperature of the right Z-wall (where the heat load is initially imposed at the channel outside) is a bit larger than that of the left Z-wall, while the average temperatures of the Y-walls coincide due to symmetry in the system (see Fig. 1). Large temperature gradients near the inlet are likely to induce significant thermal stresses and, therefore, must be carefully considered in the practical sink design in order to avoid the mechanical failure. In the analysis of the overall thermal performance of the heat sink, one should also note that the maximum increase in operating temperature does not exceed 15°C, while quite large heat fluxes of 90 W/cm^2 were successfully dissipated.

The average wall heat fluxes and the average heat

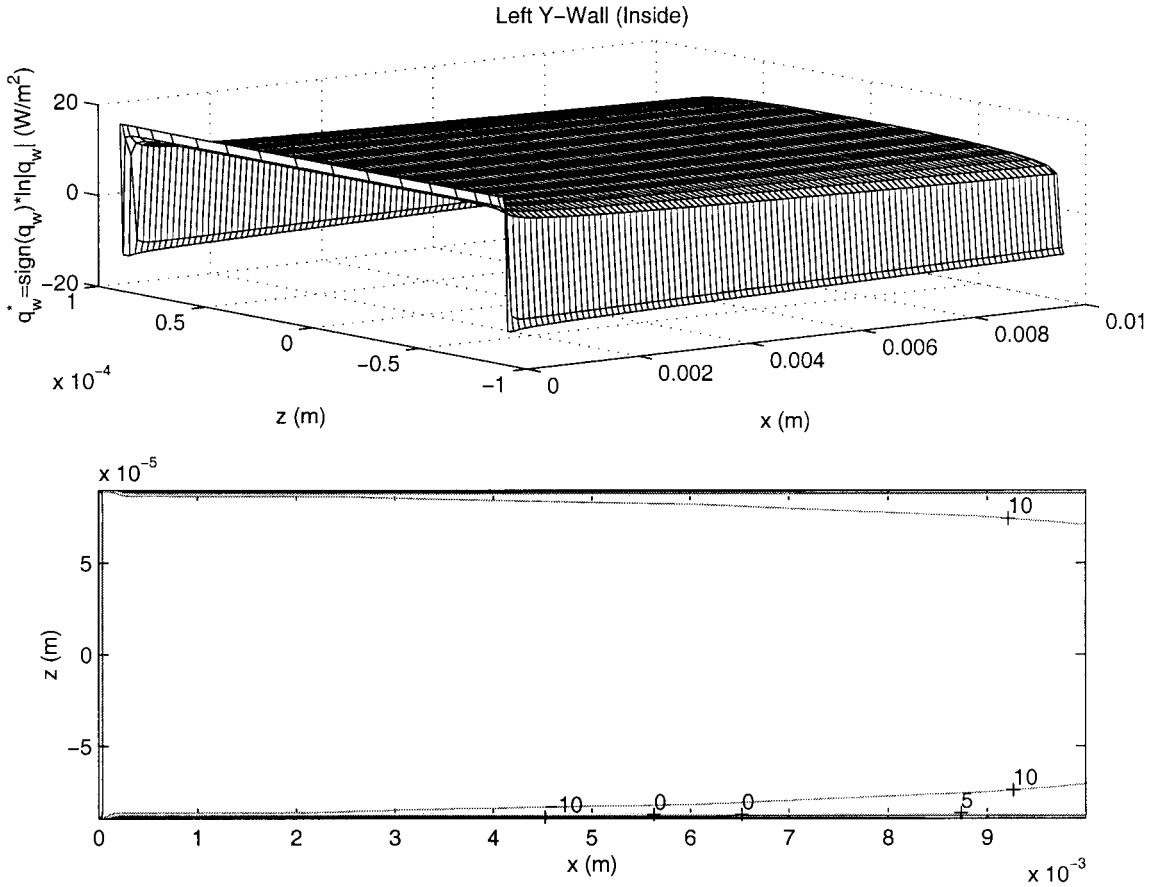

Fig. 10. Heat flux isopleths at left and right Y-walls inside the channel.

transfer coefficients are defined as

$$\bar{q}_y(x) = \int_{-H_z/2}^{H_z/2} q\big(x, y = \pm H_y/2, z\big)\,\mathrm{d}z/H_z \tag{9}$$

$$\bar{q}_z(x) = \int_{-H_y/2}^{H_y/2} q(x, y, z = \pm H_z/2)\,\mathrm{d}y/H_y \tag{10}$$

$$\bar{h}_{y,z} = \bar{q}_{y,z}/\big(\bar{T}_{y,z} - T_b\big) \tag{11}$$

respectively. As the flow develops and the boundary layers grow in the longitudinal direction, the average heat fluxes (Fig. 12) and the average heat transfer coefficients (Fig. 13) gradually decrease in magnitude. As already explained in the previous subsection in the case of the local quantities, the average heat fluxes and heat transfer coefficients are expected and, indeed, are larger at the Y-walls than at the Z-walls. Also, the magnitude of the average heat fluxes at all the four walls inside the channel is much smaller than the imposed heat flux [$q_i^* = \ln(q_i) = \ln(90 \times 10^4\ \mathrm{W/m^2}) = 13.7$] almost everywhere but in the flow development region ($x/L < 0.1$), where the heat fluxes exceed q_i significantly. This happens because the total area of the outer right Z-wall ($10^4\ \mu\mathrm{m} \times 100\ \mu\mathrm{m}$), where the heat flux q_i is imposed, is much smaller than that of the heat transfer surfaces inside the channel [$10^4\ \mu\mathrm{m} \times 2 \times (180 + 57)\ \mu\mathrm{m}$]. In addition, as discussed earlier, the upstream directed heat recirculation zones provide a physical mechanism for heat redistribution through the highly conducting silicon substrate from the downstream regions, which have the higher convective resistance than at the channel inlet.

Finally, Fig. 13 confirms that very high average heat transfer coefficients (in the order of 10 $\mathrm{kW/m^2\ K}$) can be achieved in the microchannel based heat sinks. This figure also indicates that the thermal development region is very long and occupies more than a half length of the channel (see the graphs pertinent to the Z-walls). In terms of the hydraulic diameter of the channel ($D_h = 86\ \mu\mathrm{m}$), the length of the development

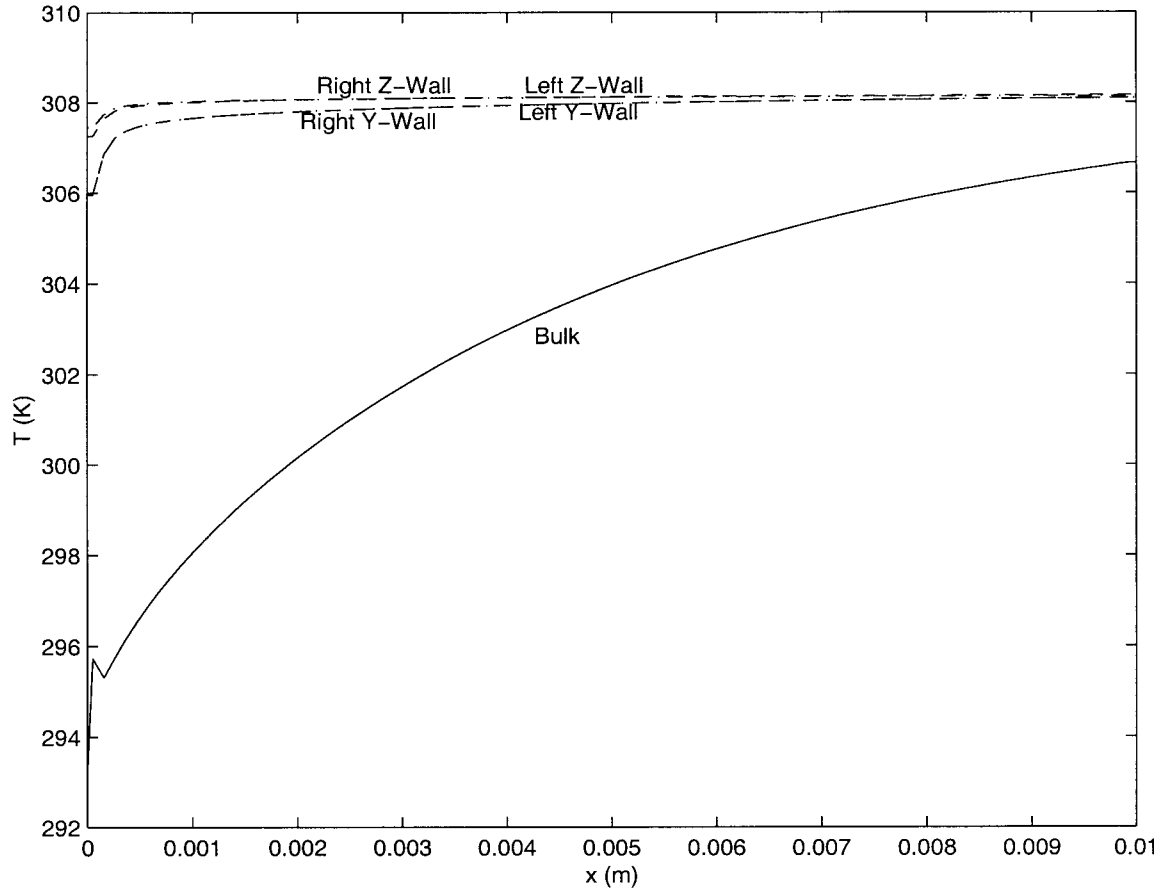

Fig. 11. Bulk and average wall temperature distributions inside the channel.

region is greater than $50 \times D_h$ if the flow Reynolds number is 140. This length increases even more for the higher Reynolds numbers.

4. Conclusion

The theoretical analysis performed, provides a fundamental understanding of the combined flow and conjugate convection–conduction heat transfer in the three-dimensional microchannel heat sink. The model formulation is general and only a few simplifying assumptions are made. Therefore, the results of the analysis as well as the conclusions can be considered as quite general and applicable to any three-dimensional conjugate heat transfer problems.

- A three-dimensional mathematical model, developed using incompressible laminar Navier–Stokes equations of motion, is capable of predicting correctly the flow and conjugate heat transfer in the microchannel heat sink. It has been validated using experimental data reported in the literature, and a good agreement has been found between the model predictions and measurements.
- The numerical results obtained, clearly demonstrate that the Poiseuille flow assumption is not always accurate, and its validity must be carefully assessed in every particular case in order to avoid significant errors in predicting the friction coefficient.
- The combined convection–conduction heat transfer in the microchannel produces very complex three-dimensional heat flow pattern with large, longitudinal, upstream directed heat recirculation zones in the highly conducting silicon substrate as well as the local, transverse heat 'vortices' in the internal corners of the channel where the fluid and solid are in direct contact. In the 'vortex' region, the local surface heat fluxes and the local convective heat transfer coefficients (Nusselt number) become negative because the bulk (mixed mean) temperature is not an appropriate reference temperature for describing the heat flow direction locally everywhere. In other

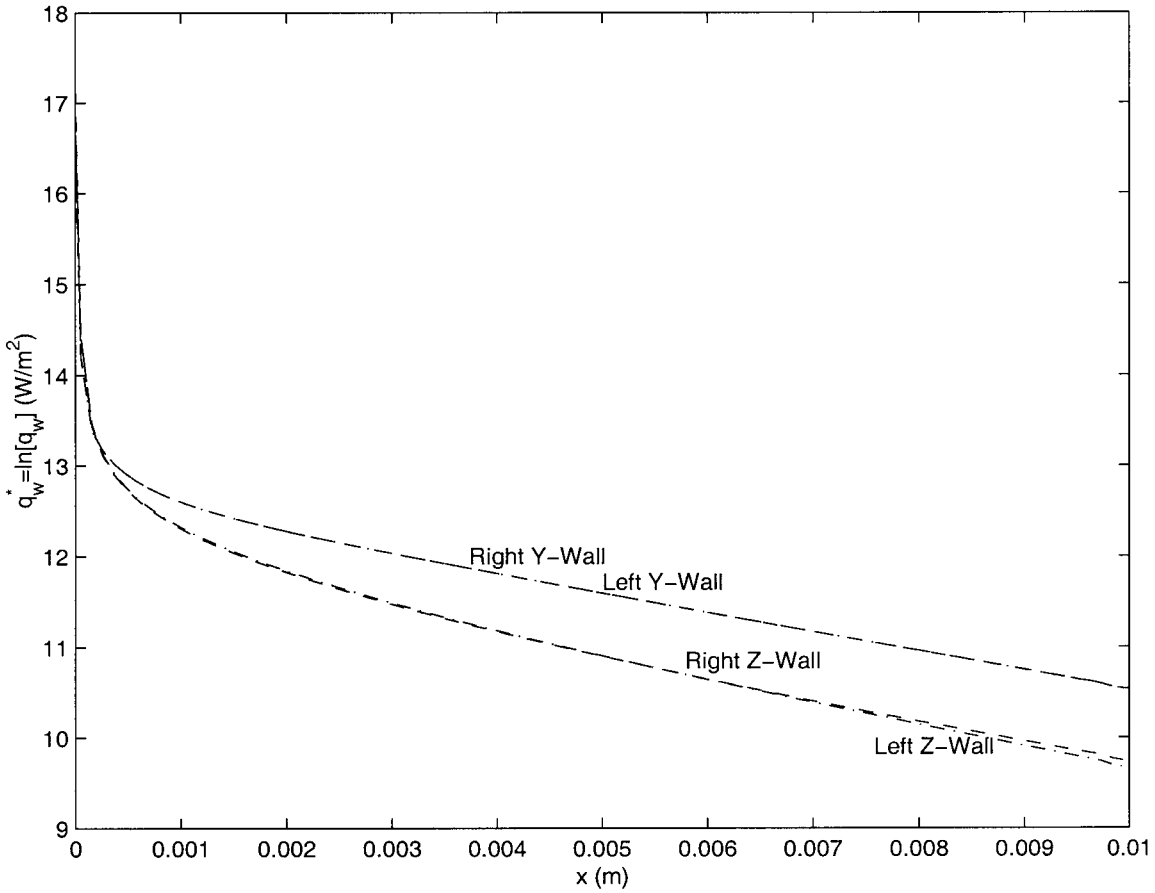

Fig. 12. Average wall heat flux distributions inside the channel.

words, the concept of the local heat transfer coefficient and Nusselt number is meaningless in the strongly conjugate problems.

- Although only the right Z-wall outside the channel is heated, the heat is redistributed by conduction within a substrate and is transferred to the coolant through all four walls inside the channel. Furthermore, the major part of the total heat input ($\approx 80\%$) is transferred to the water through the left and right Y-walls (each one contributing 40%), while only 11 and 9% is transferred through the right and left Z-walls, respectively. Such a surprising thermal energy budget is attributed to the following two factors: (1) the convective heat transfer resistance is much smaller between the closer spaced Y-walls than between the Z-walls; and (2) the total heat transfer area of the Y-walls is about three times larger than that of the Z-walls. The existing tradeoff between the combined resistances for heat spreading and heat conduction along the fin as well as the high convective resistance between the Z-walls should be addressed through geometric optimization of the specific heat sink design. Detailed parametric calculations have been performed and will be reported elsewhere due to limitations on the paper length.
- The local heat fluxes from the solid to the coolant in the small inlet region of the microchannel are larger than those in the further downstream portion by more than two orders of magnitude. This is because the average convective heat transfer coefficient is much larger in the upstream locations (the boundary layer thickness is small) and also because the highly conducting channel walls support very effective heat redistribution from the downstream (large convective resistance) to the upstream (small convective resistance) regions of the channel. This finding supports the concept of the manifold microchannel (MMC) heat sink [17,18] where the flow length is greatly reduced to small fraction of the total length of the heat sink by using a design with multiple inter-connected inlets and outlets.

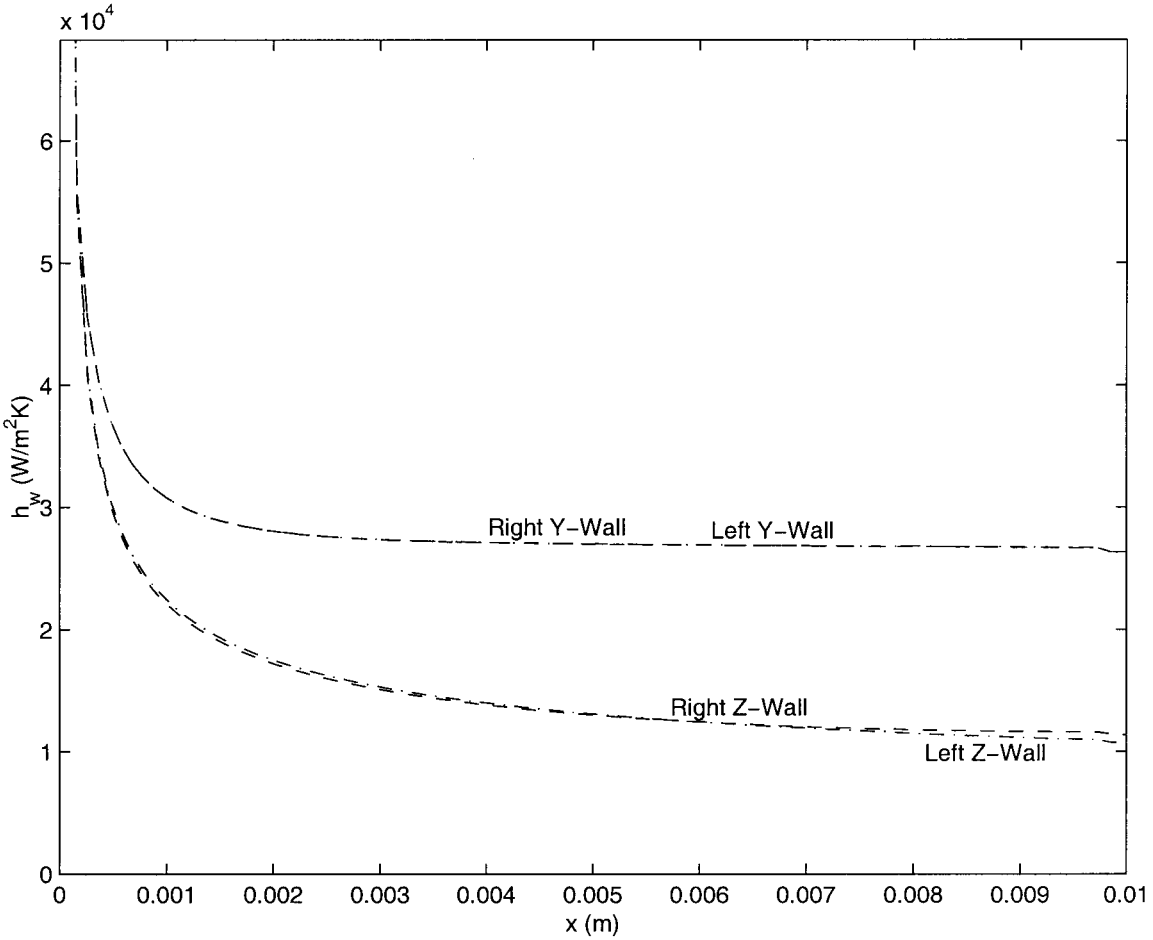

Fig. 13. Average heat transfer coefficient distributions inside the channel.

- Theoretical analysis and experimental data strongly indicate that the forced convection water cooled microchannel heat sink has a superior potential for application in thermal management of the electronic packages. The heat sink is compact and is capable of dissipating a significant thermal load (heat fluxes of the order 100 W/cm^2) with a relatively small increase in the package temperature (less than 20°C), if operated at the Reynolds numbers above 150.
- Extremely large transverse and longitudinal temperature gradients have been predicted within the solid walls in the immediate vicinity of the channel inlet. This has a potential for significant thermal stresses and structural failure of the heat sink and, therefore, must be addressed in the heat sink design by performing detailed thermomechanical calculations.

Acknowledgements

The authors are indebted to Dr. Koichiro Kawano of the Mechanical Systems Laboratory, Research and Development Center, Toshiba Corporation, Japan, for providing valuable information regarding the experimental setup for the flow and heat transfer in the microchannel heat sink which were used for validation of the theoretical model.

References

[1] R.C. Chu, G.M. Chrysler, Recent development of cooling technology and thermal design for leading-edge electronic products, International Journal of Transport Phenomena 1 (1998) 31–40.
[2] M. Mahalingam, H.M. Berg, Thermal trend in com-

ponent level packaging, International Journal of Hybrid Microelectronics 7 (1984) 1–9.
[3] M.B. Bowers, I. Mudawar, Two-phase electronic cooling using mini-channel and micro-channel heat sink, ASME Journal of Electronic Packaging 116 (1994) 290–305.
[4] P. Cheng, C.T. Hsu, A. Choudhury, Forced convection in the entrance region on a packed channel with asymmetric heating, ASME Journal of Heat Transfer 110 (1988) 946–954.
[5] T. Rizk, C. Kleinstreuer, Forced convective cooling of a linear array of blocks in open and porous matrix channels, Heat Transfer Engineering 12 (1991) 40–47.
[6] G.J. Hwang, C.H. Chao, Heat transfer measurement and analysis for sintered porous channels, ASME Journal of Heat Transfer 116 (1994) 456–464.
[7] A. Hadim, Forced convection in a porous channel with localized heat sources, ASME Journal of Heat Transfer 116 (1994) 465–472.
[8] A. Fedorov, R. Viskanta, A numerical simulation of conjugate heat transfer in an electronic package formed by embedded discrete heat sources in contact with a porous heat sink, ASME Journal of Electronic Packaging 119 (1997) 8–16.
[9] D.B. Tuckerman, R.F. Pease, High-performance heat sinking for VLSI, IEEE Electronic Devices Letters EDL-2 (1981) 126–129.
[10] D.B. Tuckerman, R.F. Pease, Optimized convective cooling using micromachined structure, Journal of Electrochemical Society 129 (1982) 98.
[11] J. Pfahler, J. Harley, H. Bau, J. Zemel, Gas and liquid flow in small channels, in: Symposium on Micromechanical Sensors, Actuators, and Systems, ASME DSC 32, 1991, pp. 49–60.
[12] S.B. Choi, R.F. Barron, R.O. Warrington, Fluid flow and heat transfer in microtubes, in: Symposium on Micromechanical Sensors, Actuators, and Systems, ASME DSC 32, 1991, pp. 123–134.
[13] K.C. Pong, C.M. Ho, Non-linear pressure distribution in microchannels, in: Proceedings of International Mechanical Engineering Congress and Exposition, vol. 197, ASME, Chicago, IL, 1994, pp. 51–56.
[14] X.F. Peng, B.X. Wang, Forced-convection and boiling characteristics in microchannels, in: Proceedings of Eleventh International Heat Transfer Conference, vol. 1, Kyongju, Korea, 1998, pp. 371–389.
[15] R.L. Webb, M. Zhang, Heat transfer and friction in small diameter channels, Microscale Thermophysical Engineering 2 (1998) 189–202.
[16] W. Nakayama, M. Behnia, D. Soodphakdee, Management of uncertainty in microchannels heat transfer. Paper presented at the Microscale Thermophysical Engineering Workshop, Kyongju, Korea, August 1998.
[17] B.C. Pak, D. Copeland, W. Nakayama, Cooling of electronic systems by using manifold microchannel heat sinks, in: Proceedings of KSME Fall Annual Meeting, vol. 2, Korea, 1995, pp. 74–80.
[18] Y.I. Kim, W.C. Chun, J.T. Kim, B.C. Pak, B.J. Back, Forced air cooling by using manifold microchannel heat sinks, KSME International Journal 12 (1998) 709–718.
[19] K. Kawano, K. Minakami, H. Iwasaki, M. Ishizuka, Development of micro channels heat exchanging, in: R.A. Nelson Jr, L.W. Swanson, M.V.A. Bianchi, C. Camci (Eds.), Application of Heat Transfer in Equipment, Systems, and Education, HTD-Vol. 361-3/PID-Vol. 3, ASME, New York, 1998, pp. 173–180.
[20] A. Weisberg, H. Bau, J. Zemel, Analysis of microchannels for integrated cooling, International Journal of Heat and Mass Transfer 35 (1992) 2465–2474.
[21] D. Yu, R. Warrington, R. Barron, T. Ameel, Experimental and theoretical investigation of fluid flow and heat transfer in microtubes, in: Proceedings of the ASME/JSME Thermal Engineering Conference, vol. 1, ASME, 1995, pp. 523–530.
[22] J.M. Li, B.X. Wang, X.F. Peng. The wall effect for laminar flow in microtubes, Molecular and Microscale Heat Transfer in Materials Processing and Other Applications, vol. 2, 1996, pp. 55–65.
[23] J.M. Li, B.X. Wang, X.F. Peng, Laminar flow of gas through extremely narrow parallel plates, in: Heat Transfer and Technology 1996, Beijing, China, 1996, pp. 318–322.
[24] G.M. Mala, D. Li, J.D. Dale, Heat transfer and fluid flow in microchannels, International Journal of Heat and Mass Transfer 40 (1997) 3079–3088.
[25] C. Yang, D. Li, J.H. Masliyah, Modeling forced liquid convection in rectangular microchannels with electrokinetic effects, International Journal of Heat and Mass Transfer 41 (1998) 4229–4249.
[26] C.S. Chen, S.M. Lee, J.D. Sheu, Numerical analysis of gas flow in microchannels, Numerical Heat Transfer, Part A 33 (1998) 749–762.
[27] A. Fedorov, R. Viskanta, Heat and mass transfer dynamics in the microchannel adsorption reactor, Microscale Thermophysical Engineering, 1998, in press.
[28] E. Eckert, R. Drake, Analysis of Heat and Mass Transfer, McGraw-Hill, New York, 1972.
[29] S.V. Patankar, Numerical Heat Transfer and Fluid Flow, Hemisphere, Washington, DC, 1980.
[30] A. Mohamad, R. Viskanta, Application of low Reynolds number k–ϵ turbulence model to buoyant and mixed flows in a shallow c cavity, in: T.S. Chen, T.Y. Chu (Eds.), Fundamentals of Mixed Convection, vol. HTD-213, ASME, New York, 1992, pp. 43–54.
[31] S. Kakaç, R. Shah, W. Aung, Handbook of Single-Phase Convective Heat Transfer, Wiley, New York, 1987.